ACS OMEGA

Article

Efficient Mineralization of Lithium Bis(pentafluoroethanesulfonyl)imide and Related Electrolyte Fluorochemicals Using Superheated Water

Hisao Hori,* Keisuke Okamura, Kaito Suzuki, and Michael Biermann

Cite This: *ACS Omega* 2024, 9, 22398−22409

Read Online

ACCESS | Metrics & More | Article Recommendations | Supporting Information

ABSTRACT: Lithium bis(pentafluoroethanesulfonyl)imide, Li[$N(SO_2C_2F_5)_2$], a typical fluorochemical aimed at better electrochemical performance of battery electrolytes, in superheated water was studied for its waste treatment. When Li[$N(SO_2C_2F_5)_2$] was reacted in pure superheated water at 300 °C, little F^- ions were produced. In contrast, complete mineralization of the fluorine, sulfur, and nitrogen atoms in Li[$N(SO_2C_2F_5)_2$] was achieved when the reaction was performed in the presence of $KMnO_4$. Specifically, when Li[$N(SO_2C_2F_5)_2$] was treated for 18 h with 158 mM of $KMnO_4$, the F^- and SO_4^{2-} yields were 101 and 99%, respectively, and the sum of the NO_3^- and NO_2^- yields was 101%. In the gas phase, trace CO_2 was detected and no CHF_3, which has high global warming potential, was formed. Furthermore, the fluorine, sulfur, and nitrogen atoms in the analogues K[$N(SO_2C_4F_9)_2$] and K[$N(SO_2CF_2)_2CF_2$] also underwent complete mineralization using the same approach.

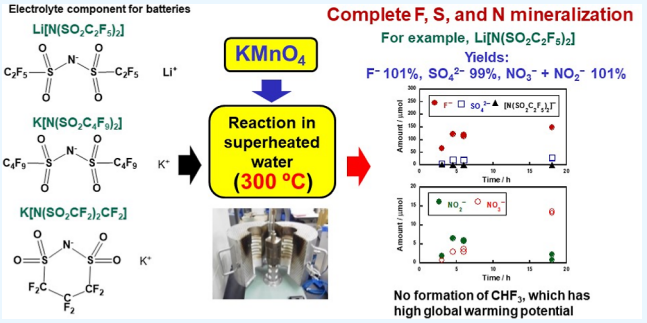

1. INTRODUCTION

Since the late 1990s, lithium bis(pentafluoroethanesulfonyl)imide, Li[$N(SO_2C_2F_5)_2$], has been widely studied as an electrolyte component for use in rechargeable lithium-ion batteries,[1−10] lithium batteries,[11−19] lithium−air batteries,[20−23] all-solid-state lithium batteries,[24−28] and so forth, because it does not only have high thermal and chemical stability but also excellent electrochemical performance: high ion conductivity, wide potential window, high cyclability, high oxygen solubility (in the case of lithium−air batteries), and high corrosion resistance, which could be useful for protecting aluminum used in positive electrodes as the current collector.[1,6,9] Li[$N(SO_2C_2F_5)_2$] is currently added to the water-in-salt electrolytes used in aqueous lithium-ion batteries to expand the potential window[29] and reduce manufacturing difficulties by improving the compatibility of the electrolyte with water and air, which enhances the safety of these batteries.[30] Li[$N(SO_2C_2F_5)_2$] certainly contributes to the safety of the electrolyte in such rechargeable batteries. However, Li[$N(SO_2C_2F_5)_2$] falls into the category of per- and polyfluoroalkyl substances (PFASs).[31] Among PFASs, perfluorooctanesulfonic acid ($C_8F_{17}SO_3H$), perfluorooctanoic acid ($C_7F_{15}COOH$), and perfluorohexanesulfonic acid ($C_6F_{13}SO_3H$) have been regulated by Stockholm Convention because of their persistence in the environment, bioaccumulation, toxicity, and mobility over long distance.[32] Furthermore, the European Chemicals Agency plans to restrict all PFASs by 2030.[33]

Under these circumstances, waste-treatment technologies that afford complete decomposition of Li[$N(SO_2C_2F_5)_2$] and its related analogues are needed. Incineration is an option to treat such fluorochemicals;[34] however, high temperatures are needed to cleave the robust carbon−fluorine bonds, and hydrogen fluoride gas is formed, which damages the firebricks of incinerators. Alternatively, if fluorine atoms in such fluorochemicals could be transformed into fluoride ions (F^-) (that is, mineralization) by means of an environmentally benign technique, the F^- ions could then be reacted with calcium hydroxide [$Ca(OH)_2$] to form calcium fluoride (CaF_2), which mineral is fluorspar. Currently, there are only a few mines globally equipped for the extraction of naturally occurring fluorspar, which is used industrially for the production of hydrofluoric acid.[35] Because hydrofluoric acid is the raw material of all fluorochemicals (carbon−fluorine bond is synthesized from carbon−chlorine bond by halogen exchange using hydrofluoric acid),[36] the development of an efficient approach for the mineralization of fluorochemicals would contribute to closing the loop of fluorine element.[37]

Received: March 3, 2024
Revised: April 16, 2024
Accepted: April 25, 2024
Published: May 8, 2024

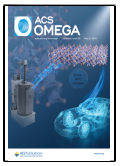

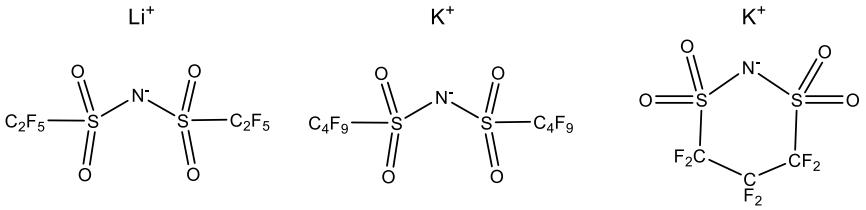

Figure 1. Structures of $Li[N(SO_2C_2F_5)_2]$ and related analogues used in this study.

Superheated (or subcritical) water is liquid water at temperatures between 100 and 374 °C (water's critical temperature). Schematic view of phase diagram of water is shown in Figure S1 in the Supporting Information. Reaction using this water is recognized as an environmentally benign technique because it has been shown to have a smaller environmental impact than pyrolysis in the recycling of nonmetallic component from electronic waste.[38] In addition, it allows generating value-added compounds.[39−43] Furthermore, unlike with pyrolysis of fluorinated compounds, even if harmful COF_2 is generated during the treatment, it is easily decomposed by hydrolysis to CO_2 and HF.[36] Of course, lowering the operation temperature and pressure are desirable in view of saving energy.

Currently, the literature contains reports on the thermal[16,44−46] and electrochemical[47,48] degradation of $Li[N(SO_2C_2F_5)_2]$. However, these previous studies have all been performed in the context of battery performance, and the level of degradation that affects battery performance is substantially lower than that required for waste treatment because the latter requires complete decomposition of the compound.

Herein, we examined the use of superheated water for the complete mineralization of $Li[N(SO_2C_2F_5)_2]$. We also applied our approach to two potassium salt analogues, one bearing $[N(SO_2C_4F_9)_2]^-$ and one bearing cyclic $[N(SO_2CF_2)_2CF_2]^-$ (Figure 1), which are also used as electrolytes and other applications.[49−52] We expect that our findings will be useful for the development of environmentally friendly industrial processes for the waste treatment of these salts.

2. EXPERIMENTAL SECTION

2.1. Reagents. $Li[N(SO_2C_2F_5)_2]$ (>98%) was purchased from Tokyo Chemical Industry (Tokyo, Japan). Potassium bis(nonafluorobutanesulfonyl)imide ($K[N(SO_2C_4F_9)_2]$) and potassium 1,1,2,2,3,3-hexafluoropropane-1,3-disulfonimide ($K[N(SO_2CF_2)_2CF_2]$) were obtained from Mitsubishi Materials Electric Chemicals (Akita, Japan). Pure argon (99.99%), oxygen (99.999%), air, and standard mixed gases CO_2 (1.00%)/N_2 and CHF_3 (0.971%)/N_2 were prepared at Taiyo Nippon Sanso (Tokyo, Japan). Other reagents were obtained from Fujifilm Wako Pure Chemical (Osaka, Japan).

2.2. Superheated Water Reactions. A representative treatment method was as follows. The reactions were conducted in a stainless-steel autoclave (35 mL volume) with a stainless-steel screw cap and a gas-sampling port. The autoclave was fitted with a gold vessel (25 mL volume, 2.8 cm i.d.) to exclude the possibility of contamination from the autoclave material. An argon-saturated aqueous solution (10 mL) of $KMnO_4$ and one of the salts ($Li[N(SO_2C_2F_5)_2]$, $K[N(SO_2C_4F_9)_2]$, or $K[N(SO_2CF_2)_2CF_2]$) were introduced into the gold vessel in the autoclave. The autoclave was pressurized with argon gas (0.6 MPa), sealed, and heated to the desired reaction temperature (250−350 °C) at a rate of 10 °C min^{-1}. After holding at the reaction temperature for the required reaction time (e.g., 6 h), the autoclave was cooled to room temperature by an air blower. The gas phase was collected through the sampling port with a sampling bag and subjected to gas chromatography/mass spectrometry (GC/MS). After collecting the gas phase, the screw cap of the autoclave was opened. The liquid−solid mixture in the gold vessel in the autoclave was collected and separated by centrifugation: the reaction solution was subjected to high-performance liquid chromatography (HPLC), ion chromatography, and HPLC/mass spectrometry (LC/MS). The collected solid was dried in vacuo and subjected to X-ray diffractometry (XRD).

2.3. Instrumental Analysis. A GC/MS system (QP2010 SE; Shimadzu, Kyoto, Japan) equipped with a fused-silica capillary column (Rt-Q-BOND; Restek, Bellefonte, PA, USA) was used for analysis of the gas-phase products. Helium was used as the carrier gas, and the injector temperature was kept constant at 120 °C. The sample gas was injected into the instrument in split mode (ratio, 20/1), and analyses were conducted in full-scan mode (m/z 2.0−200). The column oven temperature program was as follows: hold at 30 °C for 5 min, increase to 200 °C at a rate of 20 °C min^{-1}, and hold at that temperature for 20 min.

An HPLC system (IC-2010; Tosoh, Tokyo, Japan) equipped with a conductometric detector was used to quantify the amount of organic anions in the reaction solution. For $[N(SO_2C_2F_5)_2]^-$ and $[N(SO_2CF_2)_2CF_2]^-$, the analytical column was a TSKgel Super ODS-100Z (Tosoh), the eluent was a methanol−aqueous NaH_2PO_4 (20 mM, adjusted to pH 3.0 with H_3PO_4) mixture (50:50, by volume), and the flow rate was 0.8 mL min^{-1}. For $[N(SO_2C_4F_9)_2]^-$, the column and flow rate were the same, but the eluent was methanol (70 vol %) and aqueous NaH_2PO_4 (30 vol %; 20 mM, adjusted to pH 3.0 with H_3PO_4).

An ion-chromatography system (IC-8100; Tosoh) equipped with an analytical column (TSKgel Super IC-Anion HS; Tosoh) was used to quantify F^-, SO_4^{2-}, NO_3^-, and NO_2^- ions in the reaction solution. The eluent was an aqueous solution containing 7.5 mM $NaHCO_3$ and 0.8 mM Na_2CO_3 and the flow rate was 1.5 mL min^{-1}. An LC/MS system (LCMS-2010 EV; Shimadzu) equipped with a TSKgel ODS-80TSQA column (Tosoh) was used to elucidate the reaction intermediates. The mobile phase was a mixture (50:50 v/v) of methanol and an aqueous solution of ammonium acetate (1 mM, adjusted to pH 4.0 with acetic acid). The analyses were performed in negative-ion mode. XRD patterns of the collected precipitates were measured by using a MultiFlex instrument (Rigaku, Tokyo, Japan) with Cu Kα radiation.

The yields of inorganic anions, and of CO_2, were calculated based on the corresponding atom molar amount in the initial substrate (eqs 1−5)

https://doi.org/10.1021/acsomega.4c02097
ACS Omega 2024, 9, 22398−22409

$$F^- \text{ yield } (\%) = \left[\frac{(\text{moles of } F^- \text{ formed})}{(\text{moles of F atoms in initial substrate})}\right] \times 100 \quad (1)$$

$$SO_4^{2-} \text{ yield } (\%) = \left[\frac{(\text{moles of } SO_4^{2-} \text{ formed})}{(\text{moles of S atoms in initial substrate})}\right] \times 100 \quad (2)$$

$$NO_2^- \text{ yield } (\%) = \left[\frac{(\text{moles of } NO_2^- \text{ formed})}{(\text{moles of N atoms in initial substrate})}\right] \times 100 \quad (3)$$

$$NO_3^- \text{ yield } (\%) = \left[\frac{(\text{moles of } NO_3^- \text{ formed})}{(\text{moles of N atoms in initial substrate})}\right] \times 100 \quad (4)$$

$$CO_2 \text{ yield } (\%) = \left[\frac{(\text{moles of } CO_2 \text{ formed})}{(\text{moles of C atoms in initial substrate})}\right] \times 100 \quad (5)$$

3. RESULTS AND DISCUSSION

3.1. Reactivity of $Li[N(SO_2C_2F_5)_2]$. *3.1.1. Effect of $KMnO_4$ Concentration.* First, $Li[N(SO_2C_2F_5)_2]$ was heated at 300 °C for 6 h with various initial concentrations of $KMnO_4$ (0−158 mM; Figure 2), because the combination of $KMnO_4$ and superheated water is reported to promote mineralization of fluorinated compounds such as poly(vinylidene fluoride)[53] and ionic liquids.[54]

When the reaction was performed in the absence of $KMnO_4$, the amount of $[N(SO_2C_2F_5)_2]^-$ in the reaction solution decreased, but only to 7.8 μmol, which corresponded to 53% of the initial amount in $Li[N(SO_2C_2F_5)_2]$ (14.8 μmol) (Figure 2a; Table 1, entry 1). In addition, little F^- was detected (10 μmol, 7% yield) and no mineralization products (SO_4^{2-}, NO_2^-, and NO_3^-) were formed. However, when $KMnO_4$ was added to the reaction system, the amount of $[N(SO_2C_2F_5)_2]^-$ was decreased to below the detection limit, and F^-, SO_4^{2-}, NO_2^-, and NO_3^- were detected at amounts that increased with increasing $KMnO_4$ concentration (Figure 2a,b). When the $[KMnO_4]$ was 158 mM, no $[N(SO_2C_2F_5)_2]^-$ was detected and the following mineralization products were detected (averages of two replicate runs; Table 1, entry 2): F^-, 117 μmol (80% yield); SO_4^{2-}, 20 μmol (68% yield); NO_2^-, 6.0 μmol (41% yield); NO_3^-, 3.4 μmol (23% yield).

In the gas phase, only CO_2 was detected. In the absence of $KMnO_4$, 6.1 μmol of CO_2 (10% yield) was detected (Table 1, entry 1). However, in the presence of $KMnO_4$, much smaller amounts were detected, with 0.6−1.3 μmol being formed when the reactions were performed with 40−158 mM of $[KMnO_4]$ (Figure 2c). With 158 mM of $[KMnO_4]$, the average amount of CO_2 across two runs was 1.0 μmol (0% yield; Table 1, entry 2). This decrease in the formation of CO_2 was accompanied by an increase of the pH of the resulting reaction solution: in the absence of $KMnO_4$, the pH of the reaction solution was 7.9, whereas in the presence of 158 mM of $[KMnO_4]$, the pH was 12.6, which is attributed to the formation of hydroxide ions from the reaction between $KMnO_4$ and the superheated water (eq 6). At such high pH, even if CO_2 is formed, the majority of the molecules will be present in solution as CO_3^{2-}; therefore, the detection of only trace amounts of CO_2 in the gas phase is not surprising.

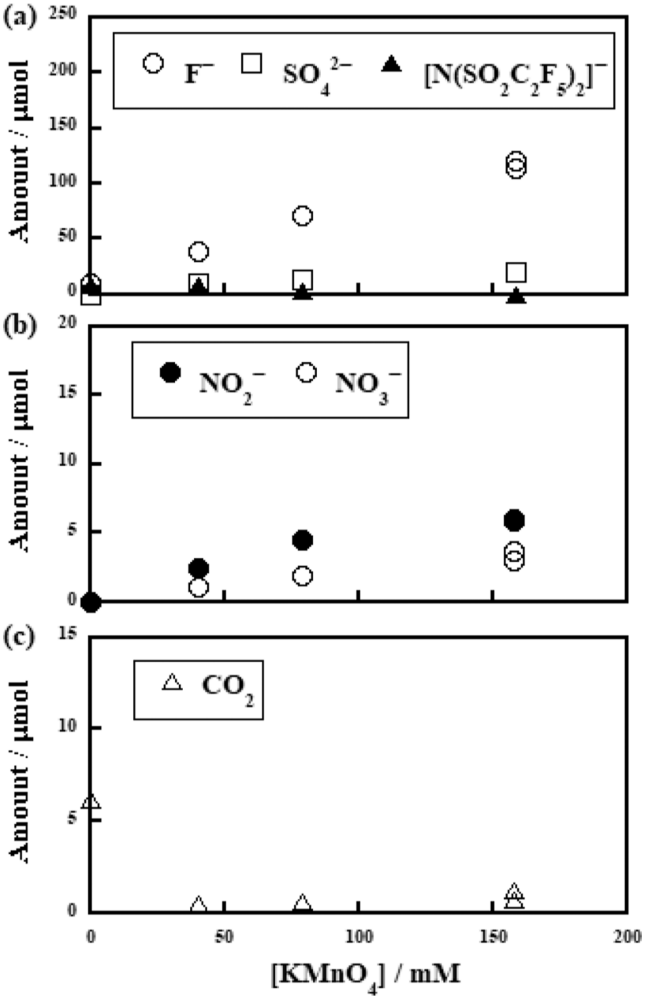

Figure 2. Initial $KMnO_4$ concentration dependences of $Li[N(SO_2C_2F_5)_2]$ decomposition. Molar amounts of (a,b) $[N(SO_2C_2F_5)_2]^-$, F^-, SO_4^{2-}, NO_2^-, and NO_3^- in the reaction solution and (c) CO_2 in the gas phase. $Li[N(SO_2C_2F_5)_2]$ (14.5−14.8 μmol) was heated with $KMnO_4$ (0−158 mM) in the presence of argon at 300 °C for 6 h. For 158 mM of $[KMnO_4]$, two replicate runs were performed.

$$4KMnO_4 + 2H_2O \rightarrow 4MnO_2 + 3O_2 + 4KOH \quad (6)$$

Next, we examined the temperature dependence of the decomposition of $Li[N(SO_2C_2F_5)_2]$ induced by 6 h treatment with 158 mM of $[KMnO_4]$ (Figure 3).

When the reaction was performed at 250 °C, 11.0 μmol of $[N(SO_2C_2F_5)_2]^-$ remained, which corresponded to 74% of the initial value, and a trace amount of F^- (1.3 μmol, 1% yield) was detected. In contrast, at 300 °C, no $[N(SO_2C_2F_5)_2]^-$ was detected in the reaction solution. The amounts of F^- and SO_4^{2-} increased with increasing temperature (Figure 3a): at 350 °C, the amounts of F^- and SO_4^{2-} were 135 μmol (91% yield) and 27.3 μmol (95% yield), respectively. The amount of NO_3^- also increased with increasing temperature; in contrast, the amount of NO_2^- increased up to 300 °C, but it then decreased at 350 °C (Figure 3b). At 350 °C, the amount of NO_3^- was 14.1 μmol (95% yield) and no NO_2^- was detected, indicating that all of the NO_2^- was oxidized to NO_3^-. Thus,

https://doi.org/10.1021/acsomega.4c02097
ACS Omega 2024, 9, 22398−22409

Table 1. Decomposition of $Li[N(SO_2C_2F_5)_2]$ and Related Fluorochemicals in Superheated Water

entry	initial substrate [amount/μmol]	initial [$KMnO_4$]/mM	coexisting gas	T/°C	P/MPa	time/h	remaining initial anion amount/μmol [ratio/%]	F^-/μmol [yield/%]	SO_4^{2-}/μmol [yield/%]	NO_2^-/μmol [yield/%]	NO_3^-/μmol [yield/%]	CO_2/μmol [yield/%]
1	$Li[N(SO_2C_2F_5)_2]$ [14.8]	0	argon	300	7.9	6	7.8 [53]	10 [7]	n.d.[a] [0]	n.d. [0]	n.d. [0]	6.1 [10]
2	$Li[N(SO_2C_2F_5)_2]$ [14.7 ± 1]	158	argon	300	8.3	6	n.d. [0]	117 ± 3 [80 ± 1]	20 ± 1 [68 ± 1]	6.0 ± 0.1 [41]	3.4 ± 0.4 [23 ± 2]	1.0 ± 0.3 [0]
3	$Li[N(SO_2C_2F_5)_2]$ [14.8]	158	argon	300	8.3	18	n.d. [0]	149 ± 1 [101]	29 ± 1 [99 ± 2]	1.5 ± 0.7 [10 ± 5]	13.5 ± 0.3 [91 ± 2]	0.6 [0]
4	$Li[N(SO_2C_2F_5)_2]$ [14.8]	158	air	300	8.2	18	n.d. [0]	140 [95]	29 [98]	1.0 [7]	13.6 [92]	0.9 [0]
5	$Li[N(SO_2C_2F_5)_2]$ [14.8]	158	oxygen	300	8.2	18	n.d. [0]	144 [97]	29 [98]	0.9 [6]	13.7 [93]	0.8 [0]
6	$Li[N(SO_2C_2F_5)_2]$ [7.4]	158	argon	300	8.2	18	n.d. [0]	74 [100]	15 [100]	0.8 [10]	6.9 [93]	1.1 [0]
7	$Li[N(SO_2C_2F_5)_2]$ [29.7]	158	argon	300	8.3	18	n.d. [0]	286 [96]	57 [95]	2.0 [7]	25.7 [88]	0.9 [0]
8	$K[N(SO_2C_4F_9)_2]$ [14.6]	0	argon	300	8.2	6	12.6 [86]	0.2 [0]	0.4 [1]	n.d. [0]	0.03 [0]	3.4 [0]
9	$K[N(SO_2C_4F_9)_2]$ [14.8]	158	argon	300	8.5	6	n.d. [0]	247 [93]	24 [81]	6.6 [45]	5.0 [34]	0.9 [0]
10	$K[N(SO_2C_4F_9)_2]$ [14.8]	158	argon	300	8.6	18	n.d. [0]	274 ± 12 [103 ± 4]	30 ± 1 [102 ± 2]	n.d. [0]	14.9 ± 0.5 [101 ± 3]	1.4 [0]
11	$K[N(SO_2C_4F_9)_2]$ [7.4]	158	argon	300	8.4	18	n.d. [0]	133 [100]	15 [100]	n.d. [0]	7.1 [97]	0.9 [0]
12	$K[N(SO_2C_4F_9)_2]$ [29.6]	158	argon	300	8.2	18	n.d. [0]	520 [98]	58 [98]	n.d. [0]	29.9 [101]	0.7 [0]
13	$K[N(SO_2CF_2)_2CF_2]$ [14.7]	158	argon	250	4.2	18	n.d. [0]	85 ± 2 [96 ± 2]	28 ± 1 [95 ± 3]	5.9 ± 0.3 [40 ± 2]	6.7 ± 0.6 [46 ± 4]	0.5 [0]
14	$K[N(SO_2CF_2)_2CF_2]$ [14.8]	158	argon	300	8.2	6	n.d. [0]	84 [95]	30 [100]	2.0 [13]	12.3 [83]	1.2 [0]

[a]n.d. = not detected.

https://doi.org/10.1021/acsomega.4c02097
ACS Omega 2024, 9, 22398−22409

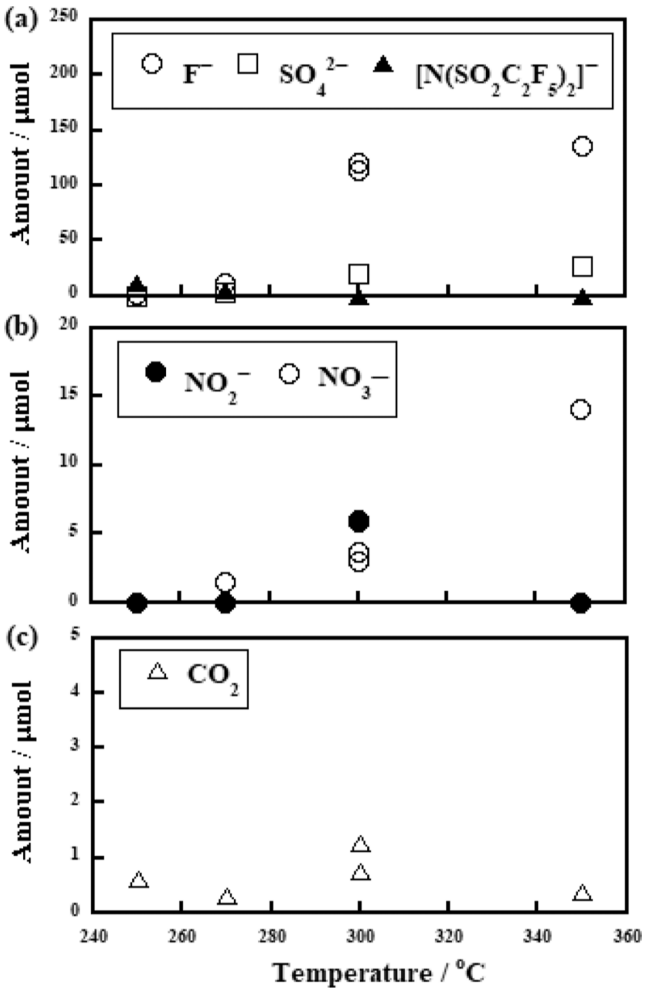

Figure 3. Reaction temperature dependences of $Li[N(SO_2C_2F_5)_2]$ decomposition. Molar amounts of (a,b) $[N(SO_2C_2F_5)_2]^-$, F^-, SO_4^{2-}, NO_2^-, and NO_3^- in the reaction solution and (c) CO_2 in the gas phase. $Li[N(SO_2C_2F_5)_2]$ (14.5−14.9 μmol) was heated with 158 mM of $[KMnO_4]$ in the presence of argon for 6 h. For 300 °C, two replicate runs were performed.

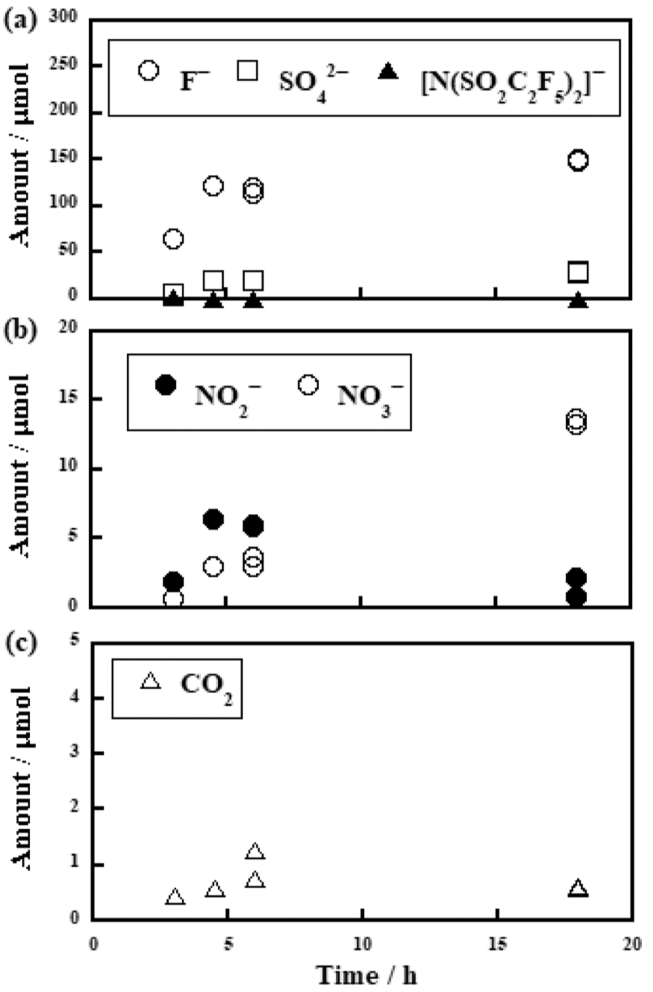

Figure 4. Reaction time dependences of the $Li[N(SO_2C_2F_5)_2]$ decomposition. Molar amounts of (a,b) $[N(SO_2C_2F_5)_2]^-$, F^-, SO_4^{2-}, NO_2^-, and NO_3^- in the reaction solution and (c) CO_2 in the gas phase. $Li[N(SO_2C_2F_5)_2]$ (14.8 μmol) was heated with 158 mM of $[KMnO_4]$ in the presence of argon at 300 °C. For 6 and 18 h, two replicate runs were performed.

the fluorine, sulfur, and nitrogen atoms in the initial $Li[N(SO_2C_2F_5)_2]$ were completely mineralized at this temperature. In the gas phase, a trace amount of CO_2 was detected (~1 μmol), and the amount remained almost constant irrespective of the increase of the reaction temperature (Figure 3c). This result is consistent with the high pH (12.6−13.1) of the resulting reaction solutions obtained from the reactions at 250−350 °C. No environmentally undesirable gases such as CHF_3, which has high global warming potential,[55] were detected in any of the runs.

3.1.2. Complete Mineralization at Lower Temperatures. To achieve complete mineralization of the fluorine, sulfur, and nitrogen atoms in $Li[N(SO_2C_2F_5)_2]$ at low temperatures, we examined extending the reaction time for the reactions at 300 °C in the presence of 158 mM of $[KMnO_4]$ (Figure 4). At 4.5 h, no $[N(SO_2C_2F_5)_2]^-$ was detected and F^- and SO_4^{2-} efficiently formed (Figure 4a). At 18 h, the amount of F^- was 149 μmol (101% yield), and the amount of SO_4^{2-} was 29 μmol (99% yield) (Table 1, entry 3, averages of two replicate runs). These results indicate that the fluorine and sulfur atoms in the initial $Li[N(SO_2C_2F_5)_2]$ were completely mineralized. For the nitrogen-containing products, the amounts NO_2^- and NO_3^- both increased up to 4.5 h, but thereafter the amount of NO_2^- decreased, and that of NO_3^- continued to increase with increasing reaction time (Figure 4b); at 18 h, the amounts of NO_2^- and NO_3^- were 1.5 μmol (10% yield) and 13.5 μmol (91% yield), respectively (Table 1, entry 3). That is, the sum of the NO_3^- and NO_2^- yields was 101%. Therefore, all of the nitrogen atoms in the initial $Li[N(SO_2C_2F_5)_2]$ were completely mineralized to NO_3^- and NO_2^-. In the gas phase, the detection of a small amount of CO_2 (below ~1 μmol, 0% yields, Figure 4c) at all time points was consistent with the high pH (12.6−12.7) of the resulting reaction solutions.

We also examined the effect of different coexisting gases. When the reaction was performed with 158 mM of $[KMnO_4]$ at 300 °C under air instead of argon, the yields of F^- and SO_4^{2-} were 95 and 98%, respectively, and the yields of NO_2^- and NO_3^- were 7 and 92%, respectively (Table 1, entry 4; sum of the yields of NO_2^- and NO_3^- was 99%). When the reaction was performed under oxygen, the yields of F^- and SO_4^{2-} were 97 and 98%, and the yields of NO_2^- and NO_3^- were 6 and 93%, respectively (Table 1, entry 5; sum of the yields of NO_2^- and NO_3^- was 99%). Thus, complete mineralization of the

https://doi.org/10.1021/acsomega.4c02097
ACS Omega 2024, 9, 22398−22409

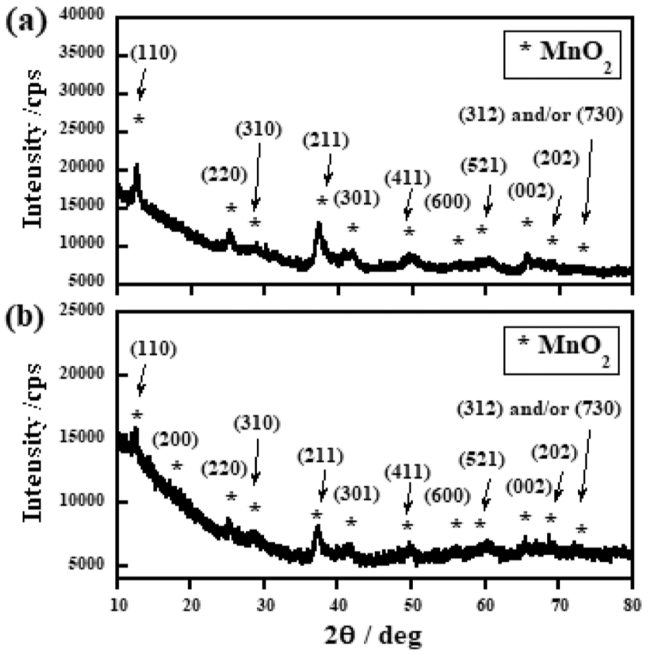

Figure 5. XRD patterns of the precipitates generated from the reactions of $Li[N(SO_2C_2F_5)_2]$ (14.8 μmol) with 158 mM of $[KMnO_4]$ in the presence of argon at 300 °C for (a) 6 h and (b) 18 h.

fluorine, sulfur, and nitrogen atoms in $Li[N(SO_2C_2F_5)_2]$ induced by $KMnO_4$ proceeds not only under argon but also under air or oxygen. Complete mineralization was also observed when the reactions were performed under argon with different amounts of $Li[N(SO_2C_2F_5)_2]$ (7.4 or 29.7 μmol), which afforded F^- yields of 100 and 96%, SO_4^{2-} yields of 100 and 95%, and total NO_2^- and NO_3^- yields of 103 and 95%, respectively (Table 1, entries 6 and 7).

3.1.3. Reaction Mechanism. To examine the fate of $KMnO_4$, the precipitates resulting from the reactions were subjected to XRD measurements (Figure 5).

When the reaction was performed with 158 mM of $[KMnO_4]$ at 300 °C for 6 or 18 h, which are conditions that afforded efficient mineralization of $Li[N(SO_2C_2F_5)_2]$, the XRD patterns of the precipitates both showed dominant peaks assignable to MnO_2. These results are consistent with the transformation of $KMnO_4$ to MnO_2 in superheated water (eq 6). The implication is that the formed MnO_2 acts as the oxidizing agent for the mineralization of $Li[N(SO_2C_2F_5)_2]$.

A plausible decomposition mechanism for the $[N(SO_2C_2F_5)_2]^-$ anion is illustrated in Scheme 1 based on the discussion below.

To detect the reaction intermediates, LC/MS analysis of the reaction solutions was performed. When the reaction was performed at 300 °C for 18 h with 158 mM of $[KMnO_4]$, which conditions $Li[N(SO_2C_2F_5)_2]$ was completely mineralized, total-ion current (TIC) mass chromatogram of the reaction solution showed one peak at a short retention time (~1.5 min) (Figure S2a of the Supporting Information). This peak (peak 1), which is from the component poorly retained on the ODS column, showed intense signals at m/z 157, 255, 353, and 451 in the mass spectrum, which were assigned to $[HSO_4 + 3HF]^-$, $[H_2SO_4 + HSO_4 + 3HF]^-$, $[2H_2SO_4 + HSO_4$

Scheme 1. Proposed Decomposition Mechanism for the $[N(SO_2C_2F_5)_2]^-$ Anion

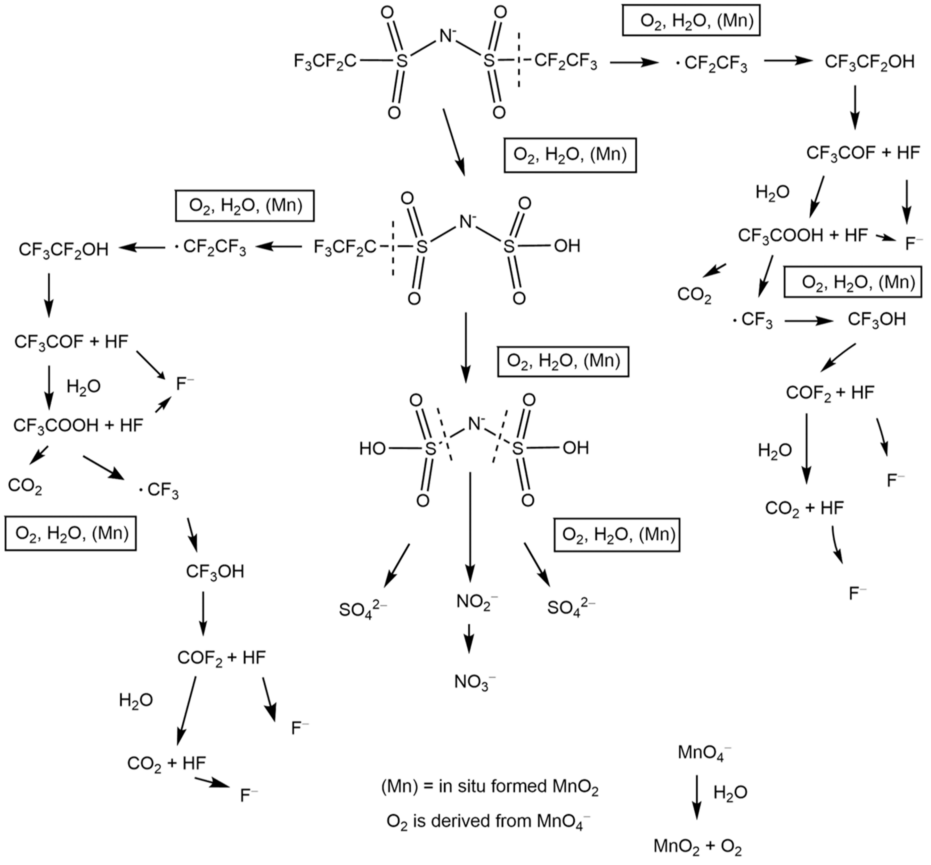

https://doi.org/10.1021/acsomega.4c02097
ACS Omega 2024, 9, 22398−22409

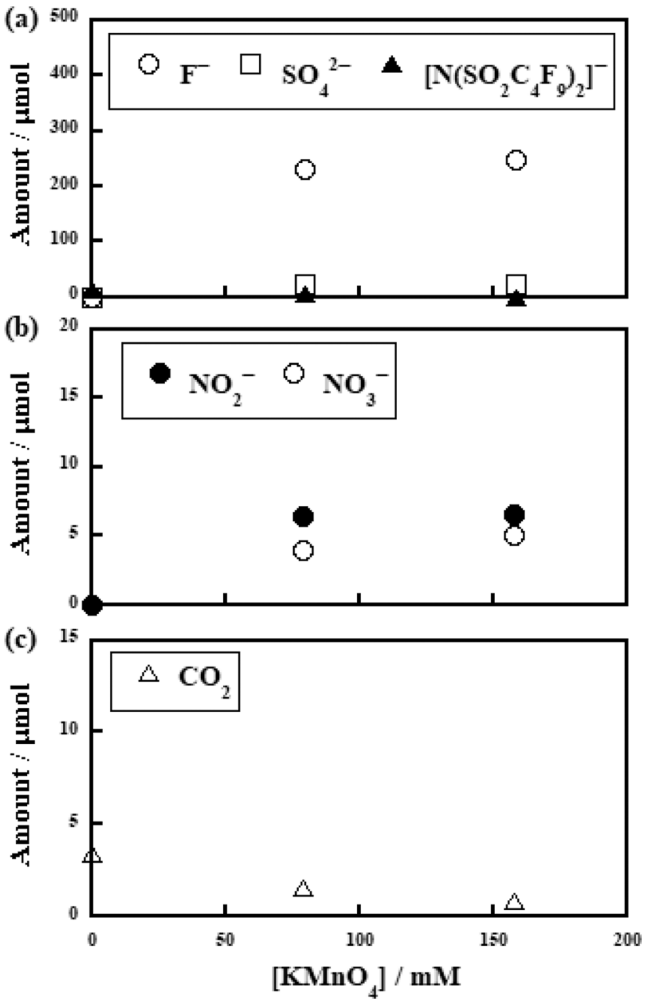

Figure 6. Initial $KMnO_4$ concentration dependences of $K[N(SO_2C_4F_9)_2]$ decomposition. Molar amounts of (a,b) $[N(SO_2C_4F_9)_2]^-$, F^-, SO_4^{2-}, NO_2^-, and NO_3^- in the reaction solution and (c) CO_2 in the gas phase. $K[N(SO_2C_4F_9)_2]$ (14.6−14.8 μmol) was heated in the presence of argon at 300 °C for 6 h.

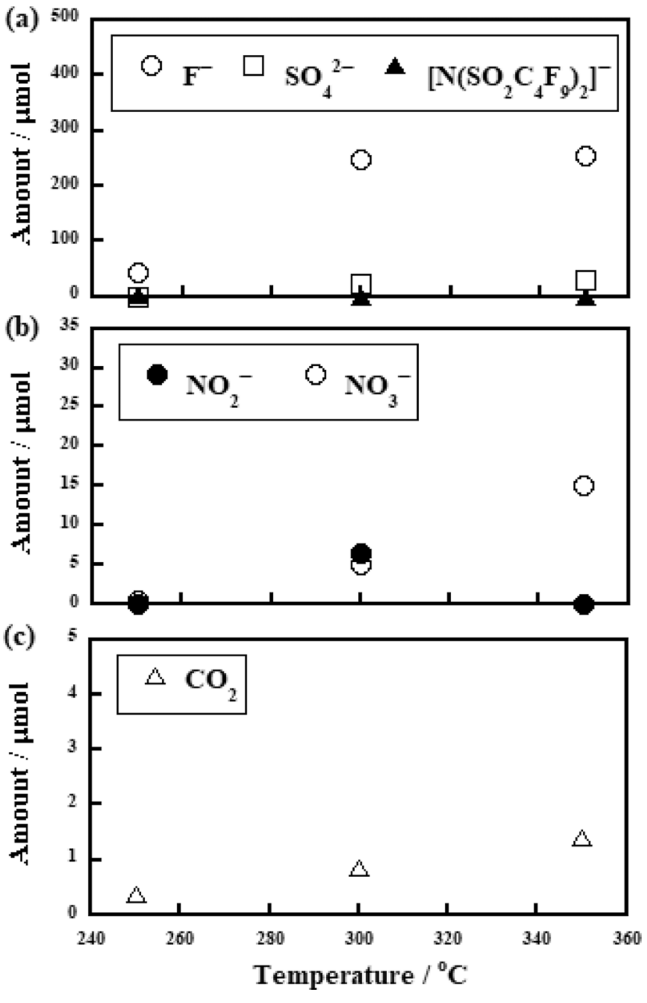

Figure 7. Reaction temperature dependences of $K[N(SO_2C_4F_9)_2]$ decomposition. Molar amounts of (a,b) $[N(SO_2C_4F_9)_2]^-$, F^-, SO_4^{2-}, NO_2^-, and NO_3^- in the reaction solution and (c) CO_2 in the gas phase. $K[N(SO_2C_4F_9)_2]$ (14.7−14.8 μmol) was heated with 158 mM of $[KMnO_4]$ in the presence of argon for 6 h.

+ $3HF]^-$, and $[3H_2SO_4 + HSO_4 + 3HF]^-$, respectively (Figure S2b). That is, the F^- and SO_4^{2-} in the reaction solution and H^+ in the acidic mobile phase generated these species at the ESI probe. However, when the reaction solution obtained under low mineralization conditions (270 °C for 6 h with 158 mM of $[KMnO_4]$; F^- yield, 8%) was examined, the TIC mass chromatogram of the reaction solution showed two peaks at ∼1.5 and ∼12 min (peaks 1 and 2 in Figure S3a, respectively). Peak 2 was at m/z 380 in the mass spectrum (Figure S3c). This m/z value corresponded to $[N(SO_2C_2F_5)_2]^-$, that is, the anion of the initial substrate, $Li[N(SO_2C_2F_5)_2]$. In contrast, peak 1 gave signals not only at m/z 157, 255, 353, and 451 (which were derived from F^- and SO_4^{2-} in the reaction solution and H^+ in the mobile phase, as described above), but also at m/z 278 (Figure S3b). This m/z value was assigned to $[C_2F_5SO_2NSO_3H]^-$. The formation of this anion indicates that decomposition of the $[N(SO_2C_2F_5)_2]^-$ was initiated by cleavage of the C−S bond, after which a C_2F_5 radical was formed. According to a traditional interpretation of oxidative PFAS degradation,[56−59] the fate of the C_2F_5 radical can be explained as follows: the radical likely reacts with O_2 (generated from eq 6) and water to form C_2F_5OH, which is unstable, to generate CF_3COF.[60] This acid fluoride is then hydrolyzed to CF_3COOH, which can oxidatively decompose to generate CF_3OH and CO_2. CF_3OH is also unstable and is transformed to HF and COF_2.[60] Finally, COF_2 is hydrolyzed to CO_2 and HF.[36] The HF results in F^- in the reaction solution. After the two C_2F_5 groups were released from the initial anion, the resulting $N(SO_3H)_2^-$ moiety is unstable, which can transform into SO_4^{2-} and NO_2^-, and NO_2^- is further oxidized to NO_3^-.

3.2. Reactivity of $K[N(SO_2C_4F_9)_2]$. Because $Li[N(SO_2C_2F_5)_2]$ was effectively mineralized by $KMnO_4$, the reactivity of $K[N(SO_2C_4F_9)_2]$, where the anion moiety has a longer perfluoroalkyl group (C_4F_9-), was examined by using the same approach. First, we examined the effect of the initial concentration of $KMnO_4$ (0−158 mM), with the reactions performed at 300 °C for 6 h (Figure 6).

In the absence of $KMnO_4$, the amount of $[N(SO_2C_4F_9)_2]^-$ was somewhat decreased (remaining ratio, 86%; Table 1, entry 8), and almost no mineralization products were detected (yields: F^-, 0%; SO_4^{2-}, 1%; NO_2^-, 0%, NO_3^-, 0%). In contrast, in the presence of $KMnO_4$, the amount of $[N(SO_2C_2F_5)_2]^-$ decreased and had completely disappeared at 158 mM of $[KMnO_4]$ (Figure 6a). In accordance with the decreasing

https://doi.org/10.1021/acsomega.4c02097
ACS Omega 2024, 9, 22398−22409

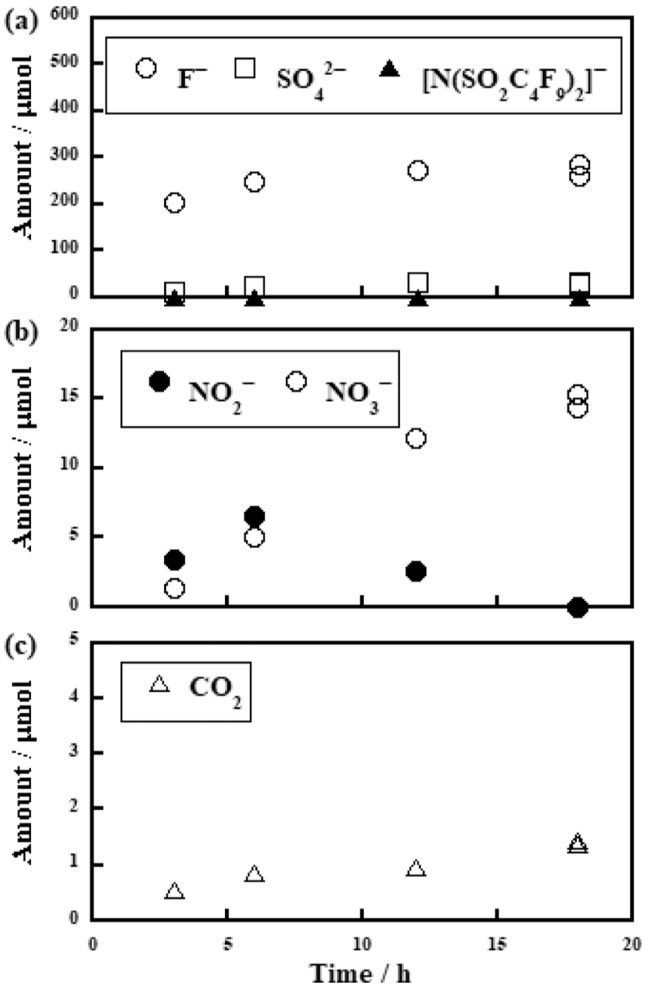

Figure 8. Reaction time dependences of $K[N(SO_2C_4F_9)_2]$ decomposition. Molar amounts of (a,b) $[N(SO_2C_4F_9)_2]^-$, F^-, SO_4^{2-}, NO_2^-, and NO_3^- in the reaction solution and (c) CO_2 in the gas phase. $K[N(SO_2C_4F_9)_2]$ (14.7−14.8 μmol) was heated with 158 mM of $[KMnO_4]$ in the presence of argon at 300 °C. For 18 h, two replicate runs were performed.

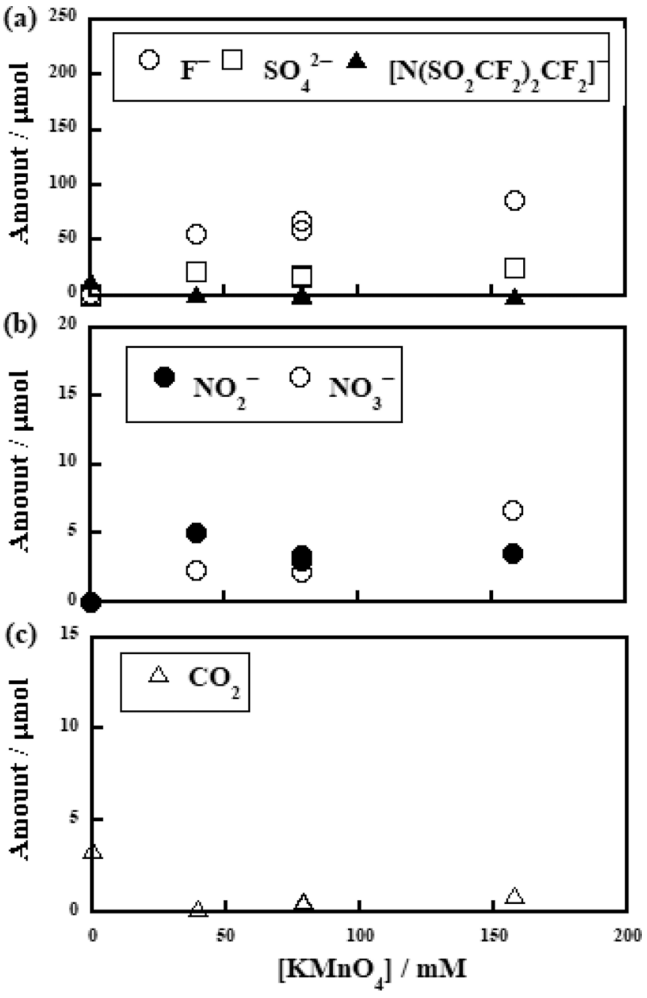

Figure 9. Initial $KMnO_4$ concentration dependences of the $K[N(SO_2CF_2)_2CF_2]$ decomposition. Molar amounts of (a,b) $[N(SO_2CF_2)_2CF_2]^-$, F^-, SO_4^{2-}, NO_2^-, and NO_3^- in the reaction solution and (c) CO_2 in the gas phase. $K[N(SO_2CF_2)_2CF_2]$ (14.7 μmol) was heated in the presence of argon at 250 °C for 6 h. For 79.0 mM of $[KMnO_4]$, two replicate runs were performed.

amount of $[N(SO_2C_2F_5)_2]^-$, the amounts of F^- and SO_4^{2-} were increased with increasing $[KMnO_4]$ (Figure 6a). The amounts of NO_2^- and NO_3^- also increased with increasing $[KMnO_4]$ (Figure 6b). When the $[KMnO_4]$ was 158 mM, the amount of F^- was 247 μmol (93% yield; Table 1, entry 9). Simultaneously, the amount of SO_4^{2-} was 24 μmol (81% yield), and those of NO_2^- and NO_3^- were 6.6 μmol (45% yield) and 5.0 μmol (34% yield), respectively. In the gas phase, like the results for $Li[N(SO_2C_2F_5)_2]$, only a small amount of CO_2 was detected, and the amount decreased with increasing $[KMnO_4]$ (Figure 6c); this is consistent with the increasing pH of the resulting reaction solutions from 5.2 to 12.5 when $[KMnO_4]$ was increased from 0 to 158 mM.

The temperature dependence of the decomposition of $K[N(SO_2C_4F_9)_2]$ was examined at 250−350 °C [6 h treatment with 158 mM of $[KMnO_4]$ (Figure 7)]. At 250 °C, the amount of $[N(SO_2C_4F_9)_2]^-$ was 2.1 μmol, which corresponded to 15% of the initial amount. Increasing the temperature to 300 °C resulted in complete disappearance of the initial anion. The amount of F^- increased with increasing temperature (Figure 7a), and at 350 °C, the amount was 255 μmol (96% yield). The amount of SO_4^{2-} also increased with increasing temperature, and at 350 °C, the amount was 29 μmol (98% yield). The amount of NO_2^- increased with increasing temperature from 250 to 300 °C, but it decreased at 350 °C (Figure 7b). In contrast, the amount of NO_3^- increased monotonically with increasing temperature. At 350 °C, the amount of NO_2^- became below the detection limit, whereas that of NO_3^- was 15.0 μmol (101% yield), indicating that NO_2^- was oxidized to NO_3^-. We conclude that the fluorine, sulfur, and nitrogen atoms in the initial $K[N(SO_2C_4F_9)_2]$ were almost completely mineralized at 350 °C. In the gas phase, only a small amount of CO_2 was detected (Figure 7c), which is consistent with the high pH of the resulting reaction solutions, although the pH did slightly decrease from 12.7 to 12.2 with increasing temperature from 250 to 350 °C.

We also examined extending the reaction time, with the aim of achieving complete mineralization of $K[N(SO_2C_4F_9)_2]$ at a lower temperature (reaction conditions: 300 °C, 158 mM of $[KMnO_4]$) (Figure 8).

No $[N(SO_2C_4F_9)_2]^-$ was detected at 3 h. The amounts of F^- and SO_4^{2-} gradually increased with increasing time (Figure 8a). At 18 h, the amount of F^- was 274 μmol (103% yield), and the amount of SO_4^{2-} was 30 μmol (102% yield) (Table 1,

https://doi.org/10.1021/acsomega.4c02097
ACS Omega 2024, 9, 22398−22409

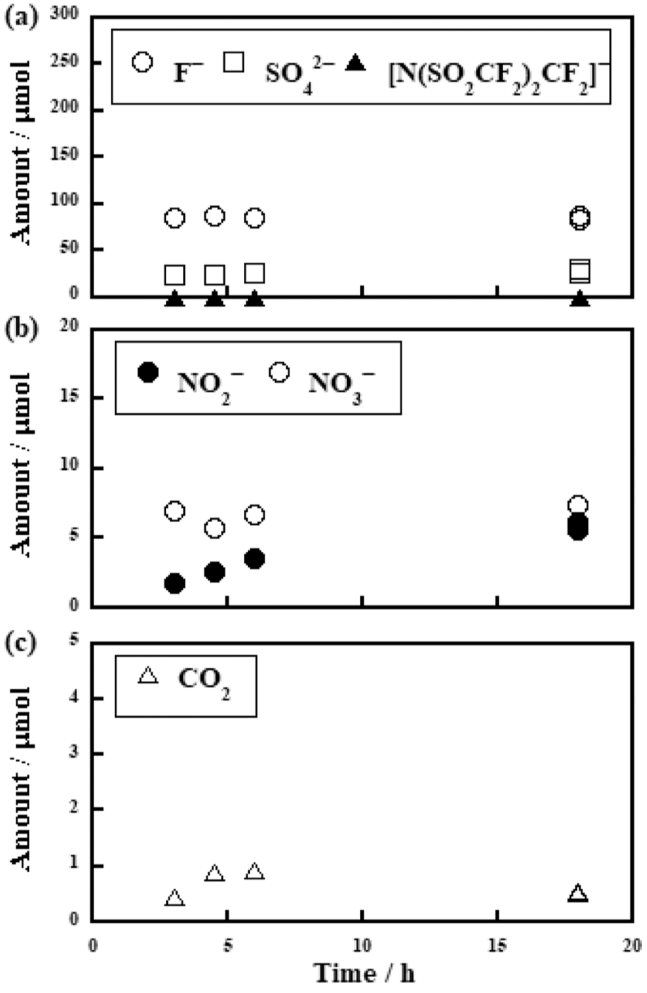

Figure 10. Reaction time dependences of $K[N(SO_2CF_2)_2CF_2]$ decomposition. Molar amounts of (a,b) $[N(SO_2CF_2)_2CF_2]^-$, F^-, SO_4^{2-}, NO_2^-, and NO_3^- in the reaction solution and (c) CO_2 in the gas phase. $K[N(SO_2CF_2)_2CF_2]$ (14.7 μmol) was heated with 158 mM of $[KMnO_4]$ in the presence of argon at 250 °C. For 18 h, two replicate runs were performed.

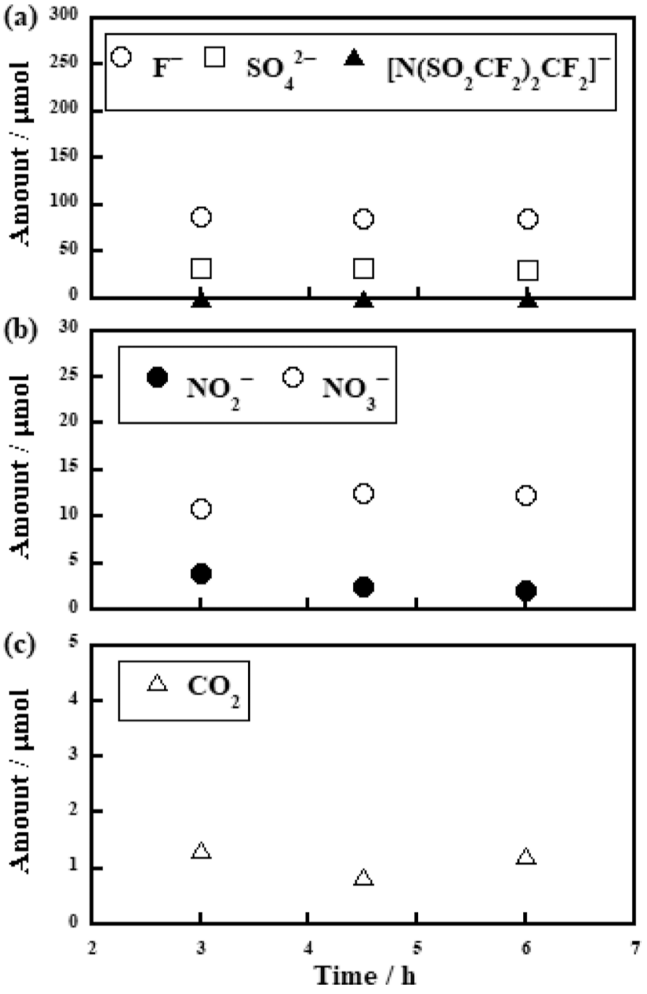

Figure 11. Reaction time dependences of $K[N(SO_2CF_2)_2CF_2]$ decomposition. Molar amounts of (a,b) $[N(SO_2CF_2)_2CF_2]^-$, F^-, SO_4^{2-}, NO_2^-, and NO_3^- in the reaction solution and (c) CO_2 in the gas phase. $K[N(SO_2CF_2)_2CF_2]$ (14.8 μmol) was heated with 158 mM of $[KMnO_4]$ in the presence of argon at 300 °C.

entry 10, averages of two replicate runs). The amount of NO_2^- increased up to 6 h and then decreased until none was detected at 18 h (Figure 8b). In contrast, the amount of NO_3^- monotonically increased with increasing reaction time. At 18 h, the amount of NO_3^- was 14.9 μmol (101% yield; Table 1, entry 10, average of two replicate runs). Thus, we conclude that almost complete mineralization of the fluorine, sulfur, and nitrogen atoms in the initial $K[N(SO_2C_4F_9)_2]$ was achieved. In the gas phase, trace CO_2 was detected as the sole product; at 18 h, the amount was 1.4 μmol (0% yield; Table 1, entry 10, average of two replicate runs). As with the results for $Li[N(SO_2C_2F_5)_2]$, the XRD patterns of the precipitates recovered from the reaction mixtures after the mineralization occurred efficiently, showed dominant peaks assignable to MnO_2 (Figure S4 in Supporting Information). Complete mineralization was also observed when the initial amount of $K[N(SO_2C_4F_9)_2]$ was changed to 7.4 or 29.6 μmol (Table 1, entries 11 and 12).

3.3. Reactivity of $K[N(SO_2CF_2)_2CF_2]$. The $K[N(SO_2CF_2)_2CF_2]$ salt, which has a cyclic $[N(SO_2CF_2)_2CF_2]^-$ anion, showed higher reactivity than $Li[N(SO_2C_2F_5)_2]$ and $K[N(SO_2C_4F_9)_2]$. Figure 9 shows the dependence of $K[N(SO_2CF_2)_2CF_2]$ decomposition on the concentration of $KMnO_4$ (reaction conditions: 250 °C, 6 h, 0−158 mM of $[KMnO_4]$). In the absence of $KMnO_4$, 13.2 μmol of $[N(SO_2CF_2)_2CF_2]^-$ remained, which corresponded to 90% of the initial value, and little F^- was detected (1.2 μmol; 1% yield). However, the amount of $[N(SO_2CF_2)_2CF_2]^-$ decreased with increasing $[KMnO_4]$, and the amount of the F^- amount also increased (Figure 9a). When the reaction was performed with 158 mM of $[KMnO_4]$, the amount of F^- was 85.7 μmol (97% yield). This yield was much higher than those obtained with $Li[N(SO_2C_2F_5)_2]$ and $K[N(SO_2C_4F_9)_2]$ under the same conditions (i.e., 1%, Figure 3a and 0%, Figure 7a, respectively). Thus, the fluorine atoms in $[N(SO_2CF_2)_2CF_2]^-$ were completely mineralized at low temperature (250 °C) by using 158 mM of $[KMnO_4]$.

Previously, we reported that $K[N(SO_2CF_2)_2CF_2]$ can be decomposed by using zerovalent iron in supercritical water at 380 °C, which afforded a maximum F^- yield of 82.5% at 18 h.[61] Thus, the present results indicate that more complete fluorine mineralization (97% F^- yield) can be achieved with the present approach at a much lower temperature (250 °C).

Although the yield of F^- was 97% with 158 mM of $[KMnO_4]$, the amount of SO_4^{2-} was 25 μmol (85%). The

https://doi.org/10.1021/acsomega.4c02097
ACS Omega 2024, 9, 22398−22409

amount of NO_2^- was increased with 39.5 mM of [$KMnO_4$], but it then decreased with increasing [$KMnO_4$], whereas the amount of NO_3^- increased with increasing [$KMnO_4$] (Figure 9b). With 158 mM of [$KMnO_4$], the amounts of NO_2^- and NO_3^- were 3.6 μmol (24% yield) and 6.8 μmol (46% yield), respectively. The sum of the NO_2^- and NO_3^- yields was 85%, indicating that reaction at 250 °C for 6 h with 158 mM of [$KMnO_4$] did not lead to complete mineralization of the sulfur and nitrogen atoms in $K[N(SO_2CF_2)_2CF_2]$. When the reactions were performed with $KMnO_4$, only trace amounts of CO_2 (0.2−0.9 μmol) were detected in the gas phase (Figure 9c), which was consistent with the high pH values (12.5−12.7) of the resulting reaction solutions.

To obtain complete mineralization of not only fluorine, but also the sulfur and nitrogen atoms in the initial $K[N(SO_2CF_2)_2CF_2]$, we examined the effect of changing the reaction time (reaction conditions: 250 °C, 158 mM of [$KMnO_4$]) (Figure 10).

No $[N(SO_2CF_2)_2CF_2]^-$ was detected at 4.5 h. F^- was efficiently formed at 3 h (84 μmol; 95% yield) (Figure 10a) and the amount remained constant out to 18 h (85 μmol, 96% yield; Table 1, entry 13, average of two runs). The amount of SO_4^{2-} was gradually increased with increasing time; at 18 h, the amount was 28 μmol (95% yield; Table 1, entry 13, average of two runs). Therefore, not only fluorine, but also the sulfur atoms in the initial $K[N(SO_2CF_2)_2CF_2]$ were almost completely mineralized. Figure 10b displays the time course of the NO_2^- and NO_3^- amounts. At 18 h the amounts of NO_2^- and NO_3^- reached 5.9 (40% yield) and 6.7 μmol (46% yield), respectively, which summed to a yield of 86%, indicating that mineralization of the nitrogen atoms in the initial substrate was incomplete. In the gas phase, only a small amount of CO_2 was detected (Figure 10c). Quasi-complete fluorine and sulfur mineralization was also observed when the initial amount of the substrate was increased threefold (i.e., to 43.9 μmol; Table S1 in the Supporting Information, where the reactions were performed at a slightly higher temperature, 255 °C for 4.5 h).

To achieve complete mineralization of all of the elements (fluorine, sulfur, and nitrogen), the reaction temperature was increased to 300 °C (Figure 11). The amounts of F^- and SO_4^{2-} were almost saturated even at 3 h (Figure 11a). At 6 h, the amounts of these anions were 84 μmol (95%) and 30 μmol (100% yield), respectively (Table 1, entry 14). The amount of NO_2^- gradually decreased with increasing time, whereas that of NO_3^- increased (Figure 11b). At 6 h, the amounts of NO_2^- and NO_3^- were 2.0 μmol (13% yield) and 12.3 μmol (83% yield), respectively (Table 1, entry 14), with the yields summing to 96%. Together, these results indicate that complete mineralization of not only in the fluorine and sulfur but also of nitrogen atoms in the initial substrate occurred. In the gas phase, only small amounts of CO_2 were detected (Figure 11c).

4. CONCLUSIONS

Here, we examined the reactions of $Li[N(SO_2C_2F_5)_2]$ in superheated water. At 300 °C, almost no mineralization of this salt was observed in pure superheated water. However, when $KMnO_4$ was added to the reaction system, complete mineralization of fluorine, sulfur, and nitrogen was observed. In the presence of 158 mM of [$KMnO_4$] (reaction conditions: 18 h, 300 °C), the yields of F^- and SO_4^{2-} were 101 and 99%, respectively, and the sum of the NO_3^- and NO_2^- yields was 101%. During these reactions, $KMnO_4$ was transformed into to MnO_2.

An analogue, $K[N(SO_2C_4F_9)_2]$, also showed complete mineralization under the same treatment conditions, allowing the yields of F^-, SO_4^{2-}, and NO_3^- of 103, 102, and 101%, respectively. Another analogue, $K[N(SO_2CF_2)_2CF_2]$, which has a cyclic $[N(SO_2CF_2)_2CF_2]^-$ anion, showed higher reactivity than both $Li[N(SO_2C_2F_5)_2]$ and $K[N(SO_2C_4F_9)_2]$. That is, under identical reaction conditions (158 mM of [$KMnO_4$], 250 °C, 6 h), the yield of F^- was 97%, whereas those for $Li[N(SO_2C_2F_5)_2]$ and $K[N(SO_2C_4F_9)_2]$ were only 1 and 0%, respectively. However, at this temperature, the mineralization of the sulfur and nitrogen atoms in $K[N(SO_2CF_2)_2CF_2]$ was incomplete. To address this, the reaction temperature was increased to 300 °C, and complete mineralization of the fluorine, sulfur, and nitrogen atoms was achieved for 6 h reaction, with yields of F^- and SO_4^{2-} of 95 and 100%, respectively, and the sum of the NO_3^- and NO_2^- yields was 96%. After these reactions, only trace amounts of CO_2 were detected in the gas phase, and no amount of CHF_3, which has high global warming potential, was detected.

■ ASSOCIATED CONTENT

Supporting Information

The Supporting Information is available free of charge at https://pubs.acs.org/doi/10.1021/acsomega.4c02097.

Schematic view of phase diagram of water; TIC mass chromatograms of the reaction solutions of $Li[N(SO_2C_2F_5)_2]$ and mass spectra of the peaks in the TIC mass chromatograms; XRD patterns of the precipitates generated from the reactions of $K[N(SO_2C_4F_9)_2]$ with 158 mM of [$KMnO_4$] under argon at 300 °C; product data obtained from reactions using higher initial amounts of $K[N(SO_2CF_2)_2CF_2]$ (PDF)

■ AUTHOR INFORMATION

Corresponding Author

Hisao Hori − *Faculty of Science, Kanagawa University, Yokohama 221-8686, Japan;* orcid.org/0000-0003-3177-5282; Email: h-hori@kanagawa-u.ac.jp

Authors

Keisuke Okamura − *Faculty of Science, Kanagawa University, Yokohama 221-8686, Japan*

Kaito Suzuki − *Faculty of Science, Kanagawa University, Yokohama 221-8686, Japan*

Michael Biermann − *Faculty of Science, Kanagawa University, Yokohama 221-8686, Japan*

Complete contact information is available at: https://pubs.acs.org/10.1021/acsomega.4c02097

Notes

The authors declare no competing financial interest.

■ ACKNOWLEDGMENTS

This work was supported by Japan Science and Technology Agency (JST) CREST grant number JPMJCR21L1.

■ REFERENCES

(1) Krause, L. J.; Lamanna, W.; Summerfield, J.; Engle, M.; Korba, G.; Loch, R.; Atanasoski, R. Corrosion of aluminum at high voltages in non-aqueous electrolytes containing perfluoroalkylsulfonyl imides;

new lithium salts for lithium-ion cells. *J. Power Sources* **1997**, *68*, 320−325.
(2) Barlowz, C. G. Reaction of water with hexafluorophosphates and with Li bis(perfluoroethylsulfonyl)imide salt. *Electrochem. Solid-State Lett.* **1999**, *2*, 362−364.
(3) Nagasubramanian, G. Comparison of the thermal and electrochemical properties of $LiPF_6$ and $LiN(SO_2C_2F_5)_2$ salts in organic electrolytes. *J. Power Sources* **2003**, *119−121*, 811−814.
(4) Gnanaraj, J. S.; Zinigrad, E.; Asraf, L.; Gottlieb, H. E.; Sprecher, M.; Aurbach, D.; Schmidt, M. The use of accelerating rate calorimetry (ARC) for the study of the thermal reactions of Li-ion battery electrolyte solutions. *J. Power Sources* **2003**, *119−121*, 794−798.
(5) Gnanaraj, J. S.; Zinigrad, E.; Levi, M. D.; Aurbach, D.; Schmidt, M. A comparison among $LiPF_6$, $LiPF_3(CF_2CF_3)_3$ (LiFAP), and $LiN(SO_2CF_2CF_3)_2$ (LiBETI) solutions: electrochemical and thermal studies. *J. Power Sources* **2003**, *119−121*, 799−804.
(6) Di Censo, D.; Exnar, I.; Graetzel, M. Non-corrosive electrolyte compositions containing perfluoroalkylsulfonyl imides for high power Li-ion batteries. *Electrochem. Commun.* **2005**, *7*, 1000−1006.
(7) Dedryvere, R.; Leroy, S.; Martinez, H.; Blanchard, F.; Lemordant, D.; Gonbeau, D. XPS valence characterization of lithium salts as a tool to study electrode/electrolyte interfaces of Li-ion batteries. *J. Phys. Chem. B* **2006**, *110*, 12986−12992.
(8) Jeong, S.-K.; Inaba, M.; Iriyama, Y.; Abe, T.; Ogumi, Z. Interfacial reactions between graphite electrodes and propylene carbonate-based solutions: Electrolyte-concentration dependence of electrochemical lithium intercalation reaction. *J. Power Sources* **2008**, *175*, 540−546.
(9) Myung, S.-T.; Yashiro, H. Electrochemical stability of aluminum current collector in alkyl carbonate electrolytes containing lithium bis(pentafluoroethylsulfonyl)imide for lithium-ion batteries. *J. Power Sources* **2014**, *271*, 167−173.
(10) Beltrop, K.; Meister, P.; Klein, S.; Heckmann, A.; Grünebaum, M.; Wiemhöfer, H. D.; Winter, M.; Placke, T. Does size really matter? New insights into the intercalation behavior of anions into a graphite-based positive electrode for dual-ion batteries. *Electrochim. Acta* **2016**, *209*, 44−55.
(11) Wang, X.; Yasukawa, E.; Mori, S. Electrochemical behavior of lithium imide/cyclic ether electrolytes for 4 V lithium metal rechargeable batteries. *J. Electrochem. Soc.* **1999**, *146*, 3992−3998.
(12) Capiglia, C.; Saito, Y.; Kageyama, H.; Mustarelli, P.; Iwamoto, T.; Tabuchi, T.; Tukamoto, H. ^{7}Li and ^{19}F diffusion coefficients and thermal properties of non-aqueous electrolyte solutions for rechargeable lithium batteries. *J. Power Sources* **1999**, *81−82*, 859−862.
(13) Wang, X.; Yasukawa, E.; Mori, S. Inhibition of anodic corrosion of aluminum cathode current collector on recharging in lithium imide electrolytes. *Electrochim. Acta* **2000**, *45*, 2677−2684.
(14) Wang, X.; Yasukawa, E.; Kasuya, S. Lithium imide electrolytes with two-oxygen-atom-containing cycloalkane solvents for 4 V lithium metal rechargeable batteries. *J. Electrochem. Soc.* **2000**, *147*, 2421−2426.
(15) Kita, F.; Sakata, H.; Sinomoto, S.; Kawakami, A.; Kamizori, H.; Sonoda, T.; Nagashima, H.; Nie, J.; Pavlenko, N. V.; Yagupolskii, Y. L. Characteristics of the electrolyte with fluoro organic lithium salts. *J. Power Sources* **2000**, *90*, 27−32.
(16) Sasaki, Y.; Handa, M.; Kurashima, K.; Tonuma, T.; Usami, K. Application of lithium organoborate with salicylic ligand to lithium battery electrolyte. *J. Electrochem. Soc.* **2001**, *148*, A999−A1003.
(17) Arai, J. A novel non-flammable electrolyte containing methyl nonafluorobutyl ether for lithium secondary batteries. *J. Appl. Electrochem.* **2002**, *32*, 1071−1079.
(18) Arai, J. Nonflammable methyl nonafluorobutyl ether for electrolyte used in lithium secondary batteries. *J. Electrochem. Soc.* **2003**, *150*, A219−A228.
(19) Jeong, S.-K.; Seo, H.-Y.; Kim, D.-H.; Han, H.-K.; Kim, J.-G.; Lee, Y. B.; Iriyama, Y.; Abe, T.; Ogumi, Z. Suppression of dendritic lithium formation by using concentrated electrolyte solutions. *Electrochem. Commun.* **2008**, *10*, 635−638.
(20) Kuboki, T.; Okuyama, T.; Ohsaki, T.; Takami, N. Lithium-air batteries using hydrophobic room temperature ionic liquid electrolyte. *J. Power Sources* **2005**, *146*, 766−769.
(21) Read, J. Ether-based electrolytes for the lithium/oxygen organic electrolyte battery. *J. Electrochem. Soc.* **2006**, *153*, A96−A100.
(22) Shah, D. B.; Olson, K. R.; Karny, A.; Mecham, S. J.; De Simone, J. M.; Balsara, N. P. Effect of anion size on conductivity and transference number of perfluoroether electrolytes with lithium salts. *J. Electrochem. Soc.* **2017**, *164*, A3511−A3517.
(23) Gittleson, F. S.; Jones, R. E.; Ward, D. K.; Foster, M. E. Oxygen solubility and transport in Li-air battery electrolytes: establishing criteria and strategies for electrolyte design. *Energy Environ. Sci.* **2017**, *10*, 1167−1179.
(24) Kim, J.- W.; Ji, K.-S.; Lee, J.-P.; Park, J.-W. Electrochemical characteristics of two types of PEO-based composite electrolyte with functional SiO_2. *J. Power Sources* **2003**, *119−121*, 415−421.
(25) Shin, J. H.; Passerini, S. PEO-$LiN(SO_2CF_2CF_3)_2$ polymer electrolytes V. Effect of fillers on ionic transport properties. *J. Electrochem. Soc.* **2004**, *151*, A238−A245.
(26) Bansal, D.; Cassel, F.; Croce, F.; Hendrickson, M.; Plichta, E.; Salomon, M. Conductivities and transport properties of gelled electrolytes with and without an ionic liquid for Li and Li-ion batteries. *J. Phys. Chem. B* **2005**, *109*, 4492−4496.
(27) Angulakshmi, N.; Prem Kumar, T.; Thomas, S.; Manuel Stephan, A. Ionic conductivity and interfacial properties of nano-chitin-incorporated polyethylene oxide-$LiN(C_2F_5SO_2)_2$ polymer electrolytes. *Electrochim. Acta* **2010**, *55*, 1401−1406.
(28) Gerbaldi, C.; Nair, J. R.; Ahmad, S.; Meligrana, G.; Bongiovanni, R.; Bodoardo, S.; Penazzi, N. UV-cured polymer electrolytes encompassing hydrophobic room temperature ionic liquid for lithium batteries. *J. Power Sources* **2010**, *195*, 1706−1713.
(29) Xie, J.; Liang, Z.; Lu, Y.-C. Molecular crowding electrolytes for high-voltage aqueous batteries. *Nat. Mater.* **2020**, *19*, 1006−1011.
(30) Yen, D.; Lin, C.-H.; Sprouster, D. J.; Zheng, X.; Xiao, X.; Lee, W.-K.; Ge, M.; Chen-Wiegart, Y. c. K. Nanotomography Investigation of 3D printed batteries with a water-in-salt gel polymer electrolyte. *ACS Mater. Lett.* **2023**, *5*, 1466−1475.
(31) Organisation for Economic Co-operation and Development (OECD). *Toward a new comprehensive global database of per- and polyfluoroalkyl substances (PFASs)*, Series on Risk Management No. 39, 2018.
(32) Stockholm Convention. All POPs listed in the Stockholm Convention. https://chm.pops.int/TheConvention/ThePOPs/AllPOPs/tabid/2509/Default.aspx (accessed on February 16, 2024).
(33) ECHA. Submitted restrictions under consideration. https://echa.europa.eu/restrictions-under-consideration/-/substance-rev/72301/term (accessed on February 16, 2024).
(34) USEPA. Technical Brief, Per- and polyfluoroalkyl substances (PFAS): Incineration to manage PFAS waste streams. https://www.epa.gov/sites/default/files/2019-09/documents/technical_brief_pfas_incineration_ioaa_approved_final_july_2019.pdf (accessed on February 16, 2024).
(35) Mineral Commodity Summaries 2023, U.S. Geological Survey, Reston, 2023; pp 70−71. https://www.usgs.gov/publications/mineral-commodity-summaries-2023 (accessed on February 16, 2024).
(36) Chambers, R. D. *Fluorine in Organic Chemistry*: Blackwell, Oxford, 2004.
(37) Schlipf, M.; Schwalm, T. Closing the recycling loop. Up-cycling of end-of-life fluoroplastics. *Kunstst. Int.* **2014**, *6*, 58−60.
(38) Wang, R.; Xu, Z. Recycling of non-metallic fractions from waste electrical and electronic equipment (WEEE): a review. *Waste Manage.* **2014**, *34*, 1455−1469.
(39) *Chemical Synthesis Using Supercritical Fluids*; Jessop, P. G., Leitner, W., Eds.; Wiley VCH: Weinheim, 1999.
(40) Peterson, A. A.; Vogel, F.; Lachance, R. P.; Fröling, M.; Antal Jr, M. J.; Tester, J. W. Thermochemical biofuel production in hydrothermal media: a review of sub- and supercritical water technologies. *Energy Environ. Sci.* **2008**, *1*, 32−65.

https://doi.org/10.1021/acsomega.4c02097
ACS Omega 2024, 9, 22398−22409

(41) Prado, J. M.; Lachos-Perez, D.; Forster-Carneiro, T.; Rostagno, M. A. Sub- and supercritical water hydrolysis of agricultural and food industry residues for the production of fermentable sugars: A review. *Food Bioprod. Process.* **2016**, *98*, 95−123.
(42) Knez, Z.; Hrncic, M. K.; Colnik, M.; Skerget, M. Chemicals and value added compounds from biomass using sub- and supercritical water. *J. Supercrit. Fluids* **2018**, *133*, 591−602.
(43) Hori, H.; Honma, R. Decomposition of fluoropolymers by their mineralization in subcritical water. In *Opportunities of Fluoropolymers*; Ameduri, B., Fomin, S., Eds.; Elsevier: Amsterdam, 2020; pp 303−331.
(44) Itoh, T.; Miyamura, Y.; Ichikawa, Y.; Uno, T.; Kubo, M.; Yamamoto, O. Composite polymer electrolytes of poly(ethylene oxide)/$BaTiO_3$/Li salt with hyperbranched polymer. *J. Power Sources* **2003**, *119*−*121*, 403−408.
(45) Kubota, K.; Nohira, T.; Hagiwara, R. Thermal properties of alkali bis(pentafluoroethylsulfonyl)amides and their binary mixtures. *J. Chem. Eng. Data* **2010**, *55*, 2546−2549.
(46) MacNeil, D. D.; Dahn, J. R. Can an electrolyte for lithium-ion batteries be too stable? *J. Electrochem. Soc.* **2003**, *150*, A21−A28.
(47) Ota, H.; Sakata, Y.; Wang, X.; Sasahara, J.; Yasukawa, E. Characterization of lithium electrode in lithium imides/ethylene carbonate and cyclic ether electrolytes. *J. Electrochem. Soc.* **2004**, *151*, A437−A446.
(48) Leroy, S.; Martinez, H.; Dedryvere, R.; Lemordant, D.; Gonbeau, D. Influence of the lithium salt nature over the surface film formation on a graphite electrode in Li-ion batteries: An XPS study. *Appl. Surf. Sci.* **2007**, *253*, 4895−4905.
(49) Conte, L.; Gambaretto, G.; Caporiccio, G.; Alessandrini, F.; Passerini, S. Perfluoroalkanesulfonylimides and their lithium salts: synthesis and characterisation of intermediates and target compounds. *J. Fluorine Chem.* **2004**, *125*, 243−252.
(50) Moriya, M.; Watanabe, T.; Sakamoto, W.; Yogo, T. Combination of organic cation and cyclic sulfonylamide anion exhibiting plastic crystalline behavior in a wide temperature range. *RSC Adv.* **2012**, *2*, 8502−8507.
(51) Xiao, Y.; Han, B.; Zeng, Y.; Chi, S.-S.; Zeng, X.; Zheng, Z.; Xu, K.; Deng, Y. New lithium salt forms interphases suppressing both Li dendrite and polysulfide shuttling. *Adv. Energy Mater.* **2020**, *10*, 1903937.
(52) Kim, H. M.; Lee, H. J.; Lee, H. K.; Hwang, T. G.; Lee, J. M.; Kim, S.; Kim, J. P. Binder-endowed thermal stability of diimmonium dye-based near-infrared (NIR) absorbing films. *Mater. Chem. Phys.* **2021**, *270*, 124773.
(53) Honma, R.; Hori, H.; da Cunha, F. R.; Horiike, N.; Steinbach, L.; Ameduri, B. Permanganate-induced efficient mineralization of poly(vinylidene fluoride) and vinylidene-fluoride based copolymers in low-temperature subcritical water. *Ind. Eng. Chem. Res.* **2019**, *58*, 13030−13040.
(54) Hori, H.; Oishi, S.; Kato, H.; Kodama, R. Complete mineralization of fluorinated ionic liquids in subcritical water in the presence of potassium permanganate. *Ind. Eng. Chem. Res.* **2020**, *59*, 5566−5575.
(55) Hodnebrog, Ø.; Etminan, M.; Fuglestvedt, J. S.; Marston, G.; Myhre, G.; Nielsen, C. J.; Shine, K. P.; Wallington, T. J. Global warming potentials and radiative efficiencies of halocarbons and related compounds: a comprehensive review. *Rev. Geophys.* **2013**, *51*, 300−378.
(56) Bentel, M. J.; Yu, Y.; Xu, L.; Li, Z.; Wong, B. M.; Men, Y.; Liu, J. Defluorination of per- and polyfluoroalkyl substances (PFASs) with hydrated electrons: structural dependence and implications to PFAS remediation and management. *Environ. Sci. Technol.* **2019**, *53*, 3718−3728.
(57) Singh, R. K.; Fernando, S.; Baygi, S. F.; Multari, N.; Thagard, S. M.; Holsen, T. M. Breakdown products from perfluorinated alkyl substances (PFAS) degradation in a plasma-based water treatment process. *Environ. Sci. Technol.* **2019**, *53*, 2731−2738.
(58) Zhuo, Q.; Deng, S.; Yang, B.; Huang, J.; Yu, G. Efficient electrochemical oxidation of perfluorooctanoate using a Ti/SnO_2-Sb-Bi anode. *Environ. Sci. Technol.* **2011**, *45*, 2973−2979.
(59) Hori, H.; Yamamoto, A.; Hayakawa, E.; Taniyasu, S.; Yamashita, N.; Kutsuna, S.; Kiatagawa, H.; Arakawa, R. Efficient decomposition of environmentally persistent perfluorocarboxylic acids by use of persulfate as a photochemical oxidant. *Environ. Sci. Technol.* **2005**, *39*, 2383−2388.
(60) Cheburkov, Y.; Lillquist, G. J. Perfluoroalcohols. *J. Fluorine Chem.* **2002**, *118*, 123−126.
(61) Hori, H.; Sakamoto, T.; Kimura, Y.; Takai, A. Iron-induced efficient mineralization of a cyclic perfluoroalkyl surfactant in subcritical and supercritical water. *Catal. Today* **2012**, *196*, 132−136.

https://doi.org/10.1021/acsomega.4c02097
ACS Omega 2024, 9, 22398−22409